Numerical integration of homogeneous functions on convex and nonconvex polygons and polyhedra

Eric B Chin, Jean B Lasserre, N Sukumar

Noname manuscript No.
(will be inserted by the editor)

Numerical integration of homogeneous functions on convex and nonconvex polygons and polyhedra

Eric B. Chin · Jean B. Lasserre · N. Sukumar

Abstract We present a method for exact integration of homogeneous functions over convex and nonconvex polygons and polyhedra. On applying Stokes's theorem and using the property of homogeneous functions, we show that it suffices to integrate these functions on the *boundary facets* of the polytope. For homogeneous polynomials, this approach is used to further reduce the integration to just function evaluations at the vertices of the polytope. This results in a cubature rule for a homogeneous polynomial f, where the integration points are only the vertices of the polytope and the function f and its partial derivatives are evaluated at these vertices. Numerical integration of homogeneous functions in polar coordinates and on curved domains are also presented. Along with an efficient algorithm for its implementation, we showcase several illustrative examples in two and three dimensions that demonstrate the accuracy of the proposed method.

Keywords numerical integration · cubature rule · Stokes's theorem · Euler's homogeneous function theorem · convex and nonconvex polytopes · weakly singular integrals

1 Introduction

Integration of polynomial functions over arbitrarily-shaped polygons or polyhedra is required in computational methods such as extended finite elements [1], embedded interface methods [2–4], virtual element method [5], and the weak Galerkin method [6] to name a few. In these applications, accurate and efficient numerical integration techniques are needed.

For integrating functions over arbitrary polytopes, three general approaches have been employed: (i) tessellation of the domain into simplices; (ii) application of generalized Stokes's theorem to reduce the volume integral to a surface integral; and (iii) use of moment fitting methods. Tessellation requires partitioning the domain into smaller subdomains (usually simplices), and then performing numerical integration over the subdomains. The generalized Stokes's theorem (Gauss's divergence theorem) converts integration over the domain into integration over the boundary of the domain, but often requires the integrand to be predefined, or requires symbolic computations. Moment fitting methods solve a linear system of equations to build a cubature rule over the domain to integrate a given set of basis functions. For further details on these three approaches, the interested reader can refer to Sudhakar et al. [3].

A technique for integrating arbitrary polynomial functions over convex polytopes was presented by Mousavi and Sukumar [7]. This method uses the properties of homogeneous functions to simplify integration over a d-dimensional arbitrary polytope to integration over the $(d-1)$-dimensional faces of the polytope. In Reference [7], cubature rules for polygons and polyhedra are constructed. However, these rules were only applied to convex polytopes, a limitation that was also noted in Reference [2]. Cubature rules that are applicable to both convex and nonconvex polytopes are desirable, and in this contribution we extend Lasserre's approach to nonconvex polytopes.

In this paper, we demonstrate that the method developed by Lasserre [8] for integrating homogeneous polynomials is also valid for nonconvex polytopes, provided a precise definition of the polytope is given. This definition of the domain of the polytope in fact broadens the utility of the method, and we provide examples that illustrate its use to integrate

National Science Foundation, CMMI-1334783.

E. B. Chin · N. Sukumar (✉)
Department of Civil and Environmental Engineering
University of Calfornia, Davis, CA, 95616, USA
E-mail: nsukumar@ucdavis.edu
J. B. Lasserre (✉)
LAAS-CNRS and Institute of Mathematics
University of Toulouse, France
E-mail: lasserre@laas.fr

homogeneous functions over a range of convex and nonconvex polygons and polyhedra. Through recursive application of Lasserre's method, we show that exact integration of homogeneous polynomials over arbitrary polytopes can be reduced to evaluation of the polynomial and its partial derivatives at the vertices of the polytope. The methods developed in this paper can be used to devise cubature rules, such as the ones constructed in Reference [7] and also elsewhere.

The remainder of this paper is organized as follows. In the following section, we establish the validity of the method described in Reference [8] for nonconvex polytopes. In Section 3, we discuss three particular extensions of this method. Specifically, in Section 3.1, we extend the method to reduce integration to function evaluation at vertices; in Section 3.2, we consider the integration of homogeneous functions over domains bounded by polar curves; and in Section 3.3, we treat the integration of weakly singular integrands and discontinuous integrands in polar coordinates over polygons. In Section 4, we provide an efficient algorithm to implement the above methods. Several numerical examples that demonstrate the accuracy and versatility of the new method are presented in Section 5, and we close with some final remarks in Section 6.

2 Integration of polynomials over arbitrary polytopes

Consider a closed polytope $P \subset \mathbb{R}^d$ on an orientable manifold whose boundary is denoted by ∂P. The boundary ∂P is defined by m $(d-1)$-dimensional *boundary facets* $\boldsymbol{F}_i$, where $\boldsymbol{F}_i \subset \boldsymbol{a}_i^T \boldsymbol{x} = b_i$ for some vectors $\boldsymbol{a}_i$ and $\boldsymbol{b}$. This definition is broader than the one used in Reference [8], since it now includes nonconvex polytopes. In comparison, a convex polytope is defined by $\boldsymbol{A}\boldsymbol{x} \leq \boldsymbol{b}$ for a matrix $\boldsymbol{A}$ of dimensions $m \times d$, and a vector $\boldsymbol{b}$ of length m. As illustrated in Figure 1, this definition is no longer valid for nonconvex polytopes, since it will erroneously include or exclude parts of the polytope P.

We wish to integrate a polynomial function, $g(\boldsymbol{x})$, over a polytope P, i.e.,

$$I = \int_P g(\boldsymbol{x})\, d\boldsymbol{x}. \tag{1}$$

For this purpose, we introduce the generalized Stokes's theorem, which can be stated as (see Reference [9]):

$$\int_P (\nabla \cdot \boldsymbol{X})\, f(\boldsymbol{x})\, d\boldsymbol{x} + \int_P \langle \boldsymbol{X}, \nabla f(\boldsymbol{x}) \rangle\, d\boldsymbol{x} = \int_{\partial P} \langle \boldsymbol{X}, \mathbf{n} \rangle\, f(\boldsymbol{x})\, d\sigma. \tag{2}$$

In (2), $\langle \cdot, \cdot \rangle$ denotes the inner product of vectors and $d\sigma$ is the Lebesgue measure on ∂P. Choosing $f(\boldsymbol{x}) := 1$ and the vector field $\boldsymbol{X} := \boldsymbol{x}$, one obtains

$$\begin{aligned} d \int_P d\boldsymbol{x} &= \sum_{i=1}^m \int_{\boldsymbol{F}_i} \left\langle \boldsymbol{x}, \frac{\boldsymbol{a}_i}{\|\boldsymbol{a}_i\|} \right\rangle d\sigma \\ &= \sum_{i=1}^m \frac{b_i}{\|\boldsymbol{a}_i\|} \int_{\boldsymbol{F}_i} d\sigma, \end{aligned} \tag{3}$$

where $d\sigma$ is the Lebesgue measure on the $(d-1)$-dimensional affine variety[1] that contains the facet $\boldsymbol{F}_i$. The formula (3), which first appeared in Reference [10], relates the volume of a polytope to the $(d-1)$-dimensional volume of its boundary, the collection of all boundary facets $\boldsymbol{F}_i$, $i = 1, \ldots, m$. Geometrically, each term of the summation can be thought of as the volume of a simplex emanating from the origin to the boundary facet, $\boldsymbol{F}_i$. In (3), b_i and $\boldsymbol{a}_i$ are related by $\boldsymbol{a}_i^T \boldsymbol{x} = b_i$, the equation of the hyperplane in which $\boldsymbol{F}_i$ lies. Furthermore, the normal to the hyperplane is: $\boldsymbol{n} = \boldsymbol{a}_i / \|\boldsymbol{a}_i\|$. This is readily verified by normalizing the gradient of $\boldsymbol{a}_i^T \boldsymbol{x}$, which is in the direction that is perpendicular to the isocontours of $\boldsymbol{a}_i^T \boldsymbol{x}$.

Let $f(\boldsymbol{x})$ be a positively homogeneous function of degree q that is continuously differentiable:

$$f(\lambda \boldsymbol{x}) = \lambda^q f(\boldsymbol{x}) \quad (\lambda > 0), \tag{4}$$

which satisfies Euler's homogeneous function theorem:

$$q f(\boldsymbol{x}) = <\nabla f(\boldsymbol{x}), \boldsymbol{x}> \quad \forall \boldsymbol{x} \in \mathbb{R}^d. \tag{5}$$

Note that for functions with degree of homogeneity $q < 0$, the validity of (5) is for $\boldsymbol{x} \in \mathbb{R}^d \backslash \{\mathbf{0}\}$. For a homogeneous function f and $\boldsymbol{X} := \boldsymbol{x}$, (2) yields

$$d \int_P f(\boldsymbol{x})\, d\boldsymbol{x} + \int_P \langle \nabla f(\boldsymbol{x}), \boldsymbol{x} \rangle\, d\boldsymbol{x} = \sum_{i=1}^m \frac{b_i}{\|\boldsymbol{a}_i\|} \int_{\boldsymbol{F}_i} f(\boldsymbol{x})\, d\sigma. \tag{6}$$

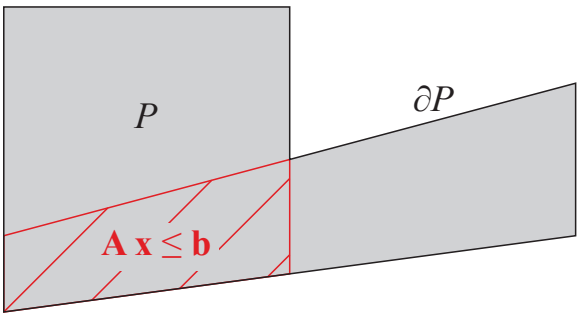

Fig. 1: An example of why $\boldsymbol{A}\boldsymbol{x} \leq \boldsymbol{b}$ does not define a nonconvex polytope. The cross-hatched region is defined by $\boldsymbol{A}\boldsymbol{x} \leq \boldsymbol{b}$ whereas the actual polygon is P (the grey, shaded area bounded by ∂P).

[1] Algebraic varieties are the extension of algebraic curves to higher dimensions, and are defined to be the set of solutions of a system of polynomial equations over real or complex numbers.

On invoking Euler's theorem given in (5), (6) simplifies to

$$\int_P f(\boldsymbol{x})\,d\boldsymbol{x} = \frac{1}{d+q}\sum_{i=1}^{m}\frac{b_i}{\|\boldsymbol{a}_i\|}\int_{\boldsymbol{F}_i} f(\boldsymbol{x})\,d\sigma. \tag{7}$$

Equation (7) relates integration of a positively homogeneous, continuously differentiable function $f(\boldsymbol{x})$ over a polytope in $\mathbb{R}^d$ to integration of the same function over the polytope's $(d-1)$-dimensional boundary, ∂P. This equation appears in Reference [8]; however, the proof therein was only valid for convex polytopes. Here, the equation applies for both convex and nonconvex polytopes, provided P is defined by its boundary facets.

The method can be extended to arbitrary polynomial functions by decomposing such a function into a collection of homogeneous polynomials, then integrating each one. More formally, consider $g(\boldsymbol{x})$ to be a polynomial of highest degree $\hat{q}$, i.e., $g(\boldsymbol{x}) := \sum_{j=0}^{\hat{q}} \hat{f}_j(\boldsymbol{x}) = \hat{f}_0(\boldsymbol{x}) + \ldots + \hat{f}_{\hat{q}}(\boldsymbol{x})$, where $\hat{f}_j(\boldsymbol{x})$ is a homogeneous polynomial of degree j. If a polynomial contains no terms of degree j, we simply have $\hat{f}_j(\boldsymbol{x}) = 0$. Now, selecting $X := \boldsymbol{x}$ and $f(\boldsymbol{x}) := g(\boldsymbol{x})$, (2) becomes

$$\int_P g(\boldsymbol{x})\,d\boldsymbol{x} = \sum_{j=0}^{\hat{q}}\frac{1}{d+j}\sum_{i=1}^{m}\frac{b_i}{\|\boldsymbol{a}_i\|}\int_{\boldsymbol{F}_i}\hat{f}_j(\boldsymbol{x})\,d\sigma. \tag{8}$$

3 Extensions of Lasserre's method

3.1 Integration on facets of lower dimensions

We further reduce the integration of $\int_{\boldsymbol{F}_i} f(\boldsymbol{x})\,d\sigma$ through application of Stokes's theorem. We define $\boldsymbol{F}_{ij} := \boldsymbol{F}_i \cap \boldsymbol{F}_j$ for $j \neq i$. $\mathcal{H}_{ij}$ is the $(d-2)$-dimensional variety that is the intersection of $\mathcal{H}_i$ and $\mathcal{H}_j$, and $\boldsymbol{n}_{ij}$ is the d-dimensional unit vector that lies in $\mathcal{H}_i$ and is normal to $\boldsymbol{F}_{ij}$. Now,

$$\boldsymbol{x} := \boldsymbol{x}_0 + \sum_{i=1}^{d-1} x_i' \boldsymbol{e}_i' \tag{9}$$

is a point in $\mathbb{R}^d$ that lies in $\mathcal{H}_i$. In (9), $\boldsymbol{x}_0 \in \mathcal{H}_i$ is an arbitrary point (serves as the origin) that satisfies $\boldsymbol{a}_i^T\boldsymbol{x}_0 = b_i$, and $\{\boldsymbol{e_i'}\}_{i=1}^{d-1}$ form an orthonormal basis on the $(d-1)$-dimensional subspace $\mathcal{H}_i$. Note that the divergence of $\boldsymbol{x}$ (restricted to $\mathcal{H}_i$) is $d-1$. For a homogeneous function $f(\boldsymbol{x})$ and choosing the vector field $\boldsymbol{X} := \boldsymbol{x} - \boldsymbol{x}_0 = \sum_{i=1}^{d-1} x_i'\boldsymbol{e}_i'$, (2) becomes

$$(d-1)\int_{\boldsymbol{F}_i} f(\boldsymbol{x})\,d\sigma + q\int_{\boldsymbol{F}_i} f(\boldsymbol{x})\,d\sigma = \sum_{i\neq j}\int_{\boldsymbol{F}_{ij}} \langle \boldsymbol{x}-\boldsymbol{x}_0, \boldsymbol{n}_{ij}\rangle\, f(\boldsymbol{x})\,d\nu + \int_{\boldsymbol{F}_i}\langle \nabla f(\boldsymbol{x}), \boldsymbol{x}_0\rangle\,d\sigma.$$

Let $d_{ij} := \langle \boldsymbol{x} - \boldsymbol{x}_0, \boldsymbol{n}_{ij}\rangle$ be the algebraic distance from $\boldsymbol{x}_0$ to $\mathcal{H}_{ij}$. Then, the above equation simplifies to

$$\int_{\boldsymbol{F}_i} f(\boldsymbol{x})\,d\sigma = \frac{1}{d+q-1}\left[\sum_{i\neq j}\int_{\boldsymbol{F}_{ij}} d_{ij} f(\boldsymbol{x})\,d\nu + \int_{\boldsymbol{F}_i}\langle \nabla f(\boldsymbol{x}), \boldsymbol{x}_0\rangle\,d\sigma\right]. \tag{10}$$

Equation (10) appears in Reference [8]; however, here it is shown to be valid for both convex and nonconvex polytopes. When $f(\boldsymbol{x})$ is a polynomial, (10) can be applied recursively to reduce integration over the polytope to evaluations of $f(\boldsymbol{x})$ and its partial derivatives at the vertices. A simple example demonstrating this reduction is provided in Section 5.

In (10), the choice of $\boldsymbol{x}_0 \in \mathcal{H}_i$ is arbitrary. However, careful selection of $\boldsymbol{x}_0$ can reduce the number of function evaluations that are required. For example, consider the function $f(\boldsymbol{x}) = x^{100}y$ defined in $\mathbb{R}^2$. If $\boldsymbol{F}_i$ is not parallel to the y-axis, choosing $\boldsymbol{x}_0$ such that it lies at the intersection of $\mathcal{H}_i$ and $x = 0$ greatly reduces the number of partial derivatives that need to be taken.

Combining (10) with (7), we can write down an explicit formula for the volume of a polytope in terms of the locations of its vertices. In 2D, this formula is:

$$\int_P f(\boldsymbol{x})\,d\boldsymbol{x} = \frac{1}{2}\sum_{i=1}^{m}\frac{b_i}{\|\boldsymbol{a}_i\|}\sum_{j\neq i} d_{ij}. \tag{11}$$

Geometrically, $\sum_{j\neq i} d_{ij}$ is the length of the boundary edge, $\boldsymbol{F}_i$, and $b_i/\|\boldsymbol{a}_i\|$ is the algebraic distance (can be positive or negative) from the origin to $\mathcal{H}_i$. Therefore, the summation can be thought of as a set of triangles, of positive and negative areas, emanating from the origin to the boundary edges.

In 3D, the volume formula is:

$$\int_P f(\boldsymbol{x})\,d\boldsymbol{x} = \frac{1}{3}\sum_{i=1}^{m}\frac{b_i}{\|\boldsymbol{a}_i\|}\frac{1}{2}\sum_{j\neq i} d_{ij}\sum_{k\neq i, k\neq j} d_{ijk}, \tag{12}$$

where

$$\sum_{k\neq i,k\neq j} d_{ijk} = \text{ length of } \boldsymbol{F}_{ij},$$

$$\frac{1}{2}\sum_{j\neq i} d_{ij}\sum_{k\neq i,k\neq j} d_{ijk} = \text{ area of } \boldsymbol{F}_i.$$

Equation (12) can be viewed as the sum of volumes of tetrahedrons, of positive and negative volumes, emanating from the origin to the boundary facets.

Let $\alpha = (\alpha_1, \alpha_2, \ldots, \alpha_n)$ be an n-tuple of nonnegative integers with absolute value $|\alpha| = \alpha_1 + \ldots + \alpha_n$. Let D be the differential operator in multiindex notation. We can use (10) with (7) to generate a closed-form expression for

the integral of $f(\boldsymbol{x})$ over P. For example, we have the following formula in 2D:

$$\int_P f(\boldsymbol{x})\,d\boldsymbol{x} = \sum_{i=1}^{m} \frac{b_i}{\|\boldsymbol{a}_i\|} \sum_{j\neq i} d_{ij} I(\boldsymbol{v}_{ij}), \tag{13a}$$

where

$$I(\boldsymbol{v}_{ij}) := \sum_{k=0}^{q} \frac{k!}{(q+2)!} Q_k(\boldsymbol{v}_{ij}), \tag{13b}$$

$$Q_k(\boldsymbol{v}_{ij}) := \sum_{|\alpha|=q-k}^{d} D^{|\alpha|} f(\boldsymbol{v}_{ij}). \tag{13c}$$

In (13), $\boldsymbol{v}_{ij}$ is the location of the vertex of the polygon that coincides with $\mathcal{H}_{ij}$. Also, when $k = q$, the final summation reduces to just the evaluation of the function $f(\boldsymbol{x})$ at $\boldsymbol{v}_{ij}$. Equation (13), which is valid for homogeneous polynomials of degree q, can be used as a cubature formula or for integrating homogeneous functions of degree q that are nonpolynomial and are differentiable at least q times. Note that this cubature is canonical in the sense that it only requires evaluations at vertices of the polygon, whereas cubature rules for polygons are specific to each particular polygon.

While the method described here provides a simple, and appealing route to reduce integration to lower-dimensional facets, it is not the only way to accomplish this task. An alternative geometric method to reduce integration to point-evaluations at the vertices of the polytope is presented in the Appendix.

3.2 Integration of homogeneous functions over domains bounded by polar curves

In Reference [11], a formula is derived that reduces integration of a homogeneous function over a d-dimensional region to an integral over its $(d-1)$-dimensional boundary surfaces, where the surfaces are described by homogeneous functions. Here, we provide a few extensions of this approach for polar curves and for homogeneous functions in polar form.

Consider a closed region $V \in \mathbb{R}^d$ bounded by m $(d-1)$-dimensional surfaces, A_i, which are described by the functions $h_i(\boldsymbol{x}) = b_i$, with $h_i(\boldsymbol{x})$ being a homogeneous function of degree p_i. We wish to integrate $f(\boldsymbol{x})$, a homogeneous function of degree q, over V. Applying (2) to the integral with $\boldsymbol{X} := \boldsymbol{x}$, we obtain [11]

$$\int_V f(\boldsymbol{x})\,d\boldsymbol{x} = \frac{1}{d+q} \sum_{i=1}^{m} \int_{A_i} \left\langle \frac{\nabla h_i}{\|\nabla h_i\|}, \boldsymbol{x} \right\rangle f(\boldsymbol{x})\,d\sigma. \tag{14}$$

Using the homogeneity of $h_i(\boldsymbol{x})$, we can simplify this to

$$\int_V f(\boldsymbol{x})\,d\boldsymbol{x} = \frac{1}{d+q} \sum_{i=1}^{m} p_i b_i \int_{A_i} \|\nabla h_i\|^{-1} f(\boldsymbol{x})\,d\sigma. \tag{15}$$

This result can be extended to a region bounded by curves, each of which can be expressed as a linear combination of homogeneous functions (for example, polynomials). First, we define $\hat{h}_i(\boldsymbol{x}) = \sum_{j=1}^{n} h_i^{(j)}(\boldsymbol{x}) = b_i$, where $\hat{h}_i(\boldsymbol{x})$ is a linear combination of n homogeneous polynomials, $h_i^{(j)}(\boldsymbol{x})$. The function $h_i^{(j)}(\boldsymbol{x})$ is homogeneous with degree $p_i^{(j)}$. Now, the result in (15) can be generalized to

$$\int_V f(\boldsymbol{x})\,d\boldsymbol{x} = \frac{1}{d+q} \sum_{i=1}^{m} \int_{A_i} \|\nabla \hat{h}_i\|^{-1} f(\boldsymbol{x}) \sum_{j=1}^{n} p_i^{(j)} h_i^{(j)}(\boldsymbol{x})\,d\sigma. \tag{16}$$

In $\mathbb{R}^2$, it may be the case that $f(\boldsymbol{x})$ is more conveniently represented in polar coordinates. An example in fracture mechanics is when $f(\boldsymbol{x})$ represents elastic stresses in the vicinity of a crack-tip – stresses are proportional to $1/\sqrt{r}$, where $r = \sqrt{x^2+y^2}$ represents the distance from the crack-tip. Note that the function $f(\boldsymbol{x})$ is homogeneous with degree $q = -\frac{1}{2}$. Even though the function is homogeneous, the method described in Section 3.1 is not exact since the partial derivatives of the function do not eventually vanish. As a result, we compute the one-dimensional line integrals in (7) using Gauss quadrature. In this section, we present a method to convert line integrals of this type to polar coordinates. After applying this transformation, the convergence rate is shown to improve for weakly singular integrands when compared to using quadrature on the Cartesian integral.

Consider a region in $\mathbb{R}^2$ that is defined by the polar curves $r = H_i(\theta)$. This curve can be described as the linear combination of two homogeneous functions:

$$\hat{h}_i(r,\theta) = r - H_i(\theta) = 0.$$

The gradient (in polar coordinates) of this function is

$$\nabla \hat{h}_i(r,\theta) = \left\langle 1, -\frac{1}{r}\frac{dH_i(\theta)}{d\theta} \right\rangle.$$

On setting $h_i^{(1)} := r$ and $h_i^{(2)} := -H(\theta)$ with $p_i^{(1)} = 1$ and $p_i^{(2)} = 0$, respectively, one can use (16) to obtain

$$\int_V f(\boldsymbol{x})\,d\boldsymbol{x} = \frac{1}{2+q} \sum_{i=1}^{m} \int_{A_i} \frac{r f\big(\boldsymbol{x}(\theta)\big) \|\langle r, \frac{dH_i(\theta)}{d\theta}\rangle\|}{\frac{1}{r}\|\langle r, -\frac{dH_i(\theta)}{d\theta}\rangle\|}\,d\theta,$$

where $d\sigma = \nabla \hat{h}_i(r,\theta) r\,d\theta$ is the differential of the arclength in terms of θ. Since $r = H_i(\theta)$, the above equation simplifies to

$$\int_V f(\boldsymbol{x})\,d\boldsymbol{x} = \frac{1}{2+q} \sum_{i=1}^{m} \int_{\alpha}^{\beta} H_i^2(\theta) f\big(\boldsymbol{x}(\theta)\big)\,d\theta, \tag{17}$$

where $\theta \in [\alpha, \beta]$ defines the polar curve and $f\big(\boldsymbol{x}(\theta)\big)$ represents $f(\boldsymbol{x})$ parameterized in terms of θ.

Equation (17) allows very accurate integration over regions whose boundary facets are described by equations of the form $r = H_i(\theta)$ where $H_i(\theta)$ can be any function given in terms of θ. The utility of (17) is demonstrated with the evaluation of the following integral:

$$I = \int_A f(r,\theta)\,dxdy, \quad f(r,\theta) = \frac{1}{\sqrt{r}}, \tag{18a}$$

where the region A (see Figure 2) is given by

$$A := \big\{r \in [0,1],\ \theta \in [0,\pi/2]\big\}. \tag{18b}$$

Direct integration yields the exact value: $I = \frac{\pi}{3}$. Note that the function $f(r,\theta)$ becomes singular at one of the vertices of the region A. The integral is also calculated using (17) on its three boundary facets. Since $b_i = 0$ on the two boundary facets that intersect the origin, the only nonzero contribution comes from the boundary facet $r = 1$. Therefore, on applying (17) to this problem, we obtain:

$$\int_A \frac{1}{\sqrt{r}} dxdy = \frac{2}{3}\int_0^{\pi/2} d\theta.$$

Since the integrand only contains a constant, one-point Gauss quadrature produces a result that is accurate to machine precision.

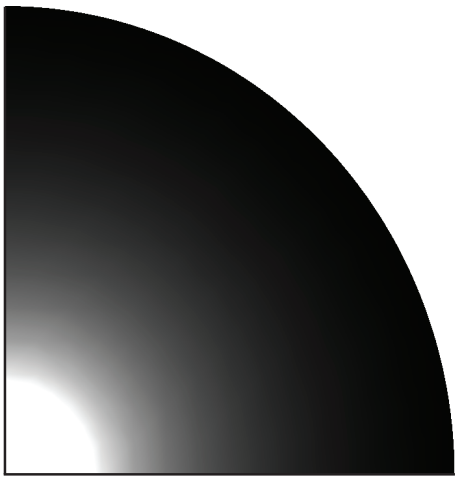

Fig. 2: The region $A := \big\{r \in [0,1],\ \theta \in [0,\pi/2]\big\}$.

The previous example, while illustrative, produced a rather trivial result. Therefore, we will also consider an example over a more complex polar region. Here, we will integrate

$$I = \int_A f(r,\theta)\,dxdy, \quad f(r,\theta) = \frac{1}{r} \tag{19a}$$

over the region A (see Figure 3), which is given by

$$A := \{r \in [0,1],\ \theta \in [\pi/4,\pi/2] : \\ r \geq \cos\theta,\ r \leq \sin\theta,\ \theta \leq \pi/2\}. \tag{19b}$$

Direct integration yields $I = \sqrt{2} - 1$. The function $1/r$ is homogeneous with degree $q = -1$. As with the previous example, a singularity is present at one of the vertices of the domain. Applying (17) to this example simplifies integration to

$$\int_A \frac{1}{r} dxdy = \int_{\pi/4}^{\pi/2} (\sin\theta - \cos\theta)\,d\theta.$$

Using a six-point Gauss rule to compute the one-dimensional integral on the right-hand side results in a relative error of 10^{-15}. The plot of the relative error as a function of the number of Gauss points is shown in Figure 3.

3.3 Integration of homogeneous functions in polar form on polygons

In the previous section, we limited the boundary of polar regions to the equation $r = H_i(\theta)$. At first glance, this may seem to limit the utility of (17). However, we demonstrate in this section that this representation for the boundary of a polar region can describe any polygon in $\mathbb{R}^2$.

The equation $\boldsymbol{a}_i^T\boldsymbol{x} = b_i$ gives the general equation of a line. Substituting $x = r\cos\theta$ and $y = r\sin\theta$ in the general equation of a line gives

$$r = \frac{b_i}{\langle \boldsymbol{a}_i, \{\cos\theta, \sin\theta\}\rangle} = \frac{b_i}{\hat{H}_i(\theta)} \tag{20}$$

where $\hat{H}_i(\theta) = \langle \boldsymbol{a}_i, \{\cos\theta, \sin\theta\}\rangle$. This polar representation of a line is of the form introduced in Section **??**, namely $r = H_i(\theta)$. Replacing (20) in (17) one obtains

$$\int_P f(\boldsymbol{x})\,dxdy = \frac{1}{2+q}\sum_{i=1}^{m} b_i^2 \int_\alpha^\beta \frac{f\big(\boldsymbol{x}(\theta)\big)}{\hat{H}_i^2(\theta)} d\theta, \tag{21}$$

where $\alpha = \tan^{-1}\frac{y_1}{x_1}$, $\beta = \tan^{-1}\frac{y_2}{x_2}$, and (x_1,y_1) and (x_2,y_2) are the vertices that lie in the domain of the boundary facet (in Cartesian coordinates). Note that if we have $f(r) = r^q \equiv f(\theta) = \big(b_i/\hat{H}_i(\theta)\big)^q$ ($q > -2$ in $\mathbb{R}^2$), then (21) simplifies to

$$\int_P f(\boldsymbol{x})\,dxdy = \frac{1}{2+q}\sum_{i=1}^{m} b_i^{q+2} \int_\alpha^\beta \frac{1}{\hat{H}_i^{q+2}(\theta)}\,d\theta. \tag{22}$$

For this technique, Gauss cubature is tested for three different functions. In the first two cases, the weakly singular integrands $f(r) = r^{-1}$ and $f(r) = r^{-1/2}$ are integrated over hexagonal and square domains. In the third

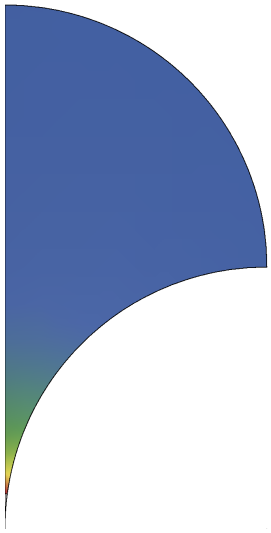

(a)

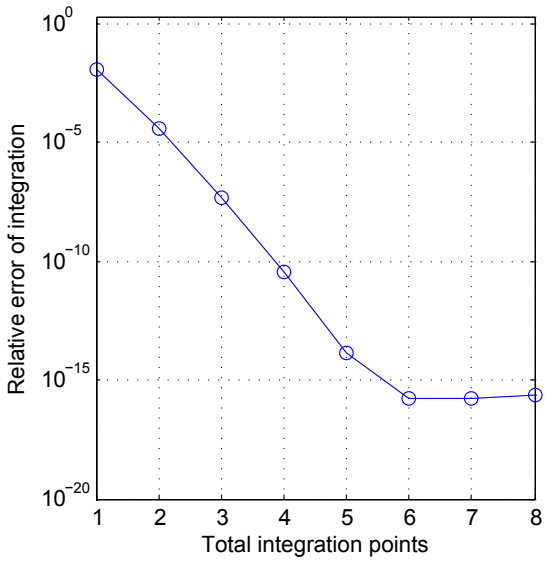

(b)

Fig. 3: Example using (17) to reduce integration to the boundary of a domain. The domain of integration A, which is given in is shown in (a) and relative error of Gauss cubature is presented in (b).

case, we consider the discontinuous, weakly singular function $f(r,\theta) = \frac{1}{\sqrt{r}} \sin \frac{\theta}{2}$. For all cases, results using cubature on the polar transformed integral $\big($given in (22)$\big)$ are compared to cubature on the untransformed Cartesian integral $\big($given in (7)$\big)$ and to tensor-product cubature, where possible.

First, we apply Gauss cubature on (22) to integrate $f(r) = r^{-1}$ and $f(r) = r^{-1/2}$ over a regular hexagon inscribed inside a unit circle centered at the origin. These functions are unbounded at the origin, but the integrals are finite and continuous, and are referred to as being weakly singular. Results are compared to those obtained using Gauss cubature on (7). As presented in Figure 4, Gauss cubature on the polar transformed integral converges more quickly than than cubature performed on (7).

Next, we apply cubature of these integrals to a bi-unit square centered at the origin. In this case, we are able to compare cubature using the techniques in this paper to tensor-product cubature. For tensor-product cubature, the domain is subdivided into four squares in each quadrant to ensure all sampling points are of finite value. While cubature on the polar integral is able to obtain precision on the order of 10^{-14} with about 55 cubature points in both cases, cubature on the Cartesian integral requires up to 75 cubature points to realize the same accuracy. Full tensor-product cubature is carried out with over 10^4 cubature points and is only accurate to 10^{-3} for $f(r) = 1/r$. Results are presented in Figure 5.

Finally, cubature of the weakly singular, discontinuous function $f(r,\theta) = \frac{1}{\sqrt{r}} \sin \frac{\theta}{2}$ is demonstrated over the bi-unit square centered at $x, y = (0.5, 0.5)$. The discontinuity in the function is treated as two additional boundary facets, and therefore, the entire domain is viewed as a nonconvex polygon with seven sides. This decomposition is demonstrated in Figure 6a. Since the tensor-product cubature points do not coincide with the location of the singularity in this case, the domain does not require subdivision. As with the previous two cases, integration of the polar transformed version of the integral provides the best results. A complete set of results for this case are plotted in Figure 6b.

4 Numerical implementation

In this section, we describe an algorithm to implement the methods detailed in Section 2 and 3.1. The assumed inputs of this algorithm are the vertices of a polytope (given in Cartesian coordinates), the connectivity of the vertices in the polytope that define the boundary facets, and the polynomial function to integrate. The output is the integral of the polynomial function over the polytope.

Algorithms 1 and 2 contain pseudocode that implements the methods and equations described in Section 2 and 3.1, respectively. Lines of pseudocode without an explicit assignment operator refer to functions that carry out the calculations described. Since implementation of the majority of these functions is straightforward, for the most part, they are not detailed in this paper.

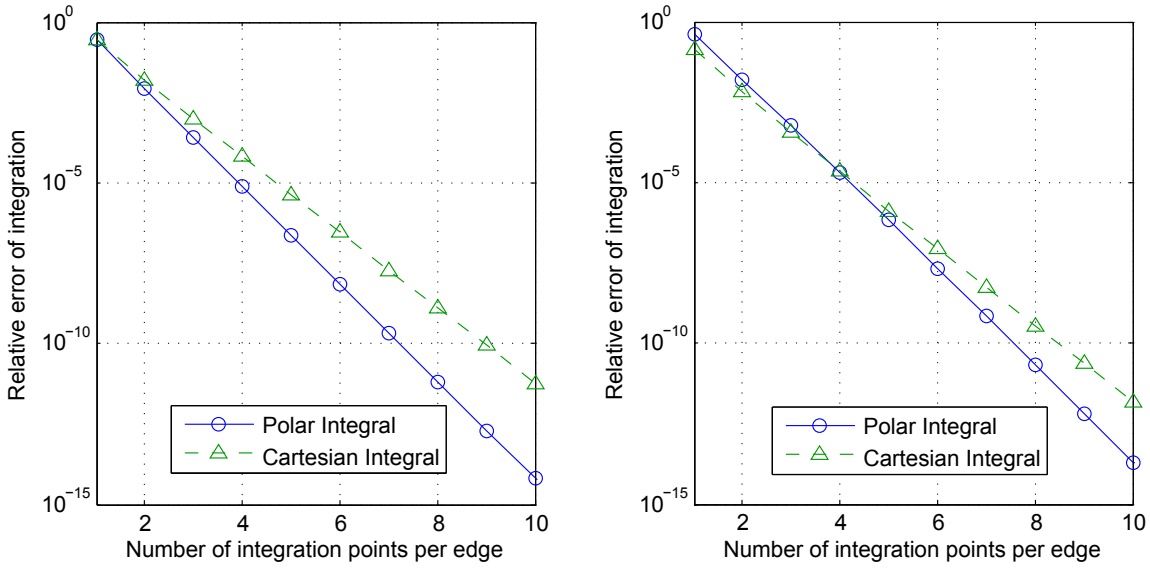

(a) $q = -1$ (b) $q = -\frac{1}{2}$

Fig. 4: Error in numerical integration of weakly singular functions over a regular hexagon that is inscribed within the unit circle. (a) $f(r) = r^{-1}$; and (b) $f(r) = r^{-1/2}$. In both plots, the dotted line with triangular markers represents cubature error with the Cartesian integral, whereas the solid line with circular markers represents cubature error for the polar integral.

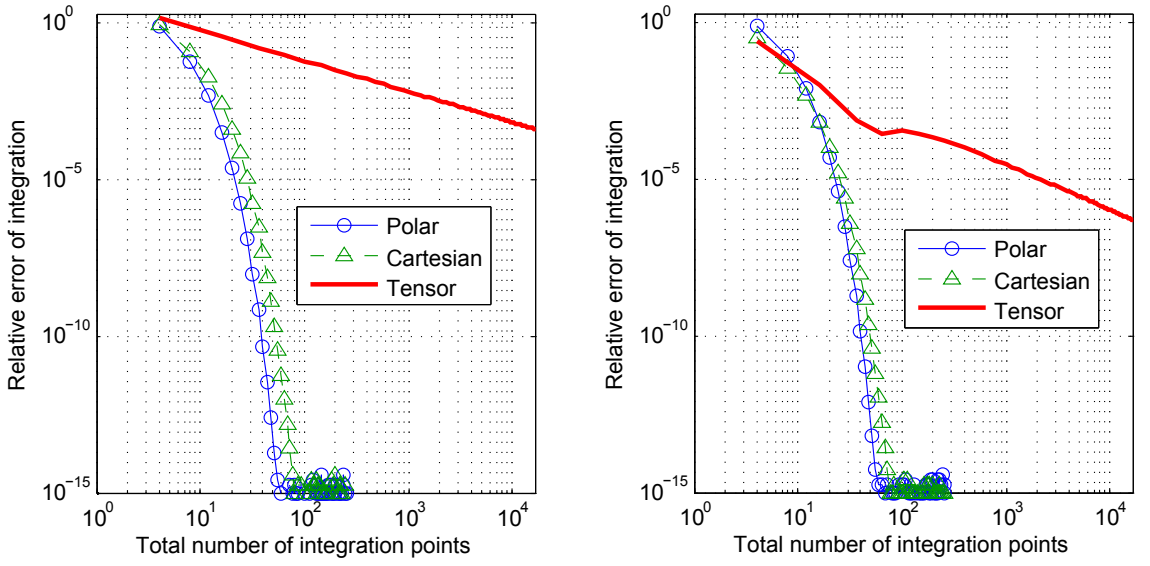

(a) $q = -1$ (b) $q = -\frac{1}{2}$

Fig. 5: Error in numerical integration of weakly singular functions over a biunit square centered at the origin. (a) $f(r) = r^{-1}$; and (b) $f(r) = r^{-1/2}$. The polar and Cartesian integrals are displayed as in Figure 4. Tensor-product cubature on the full square is shown as a thick line.

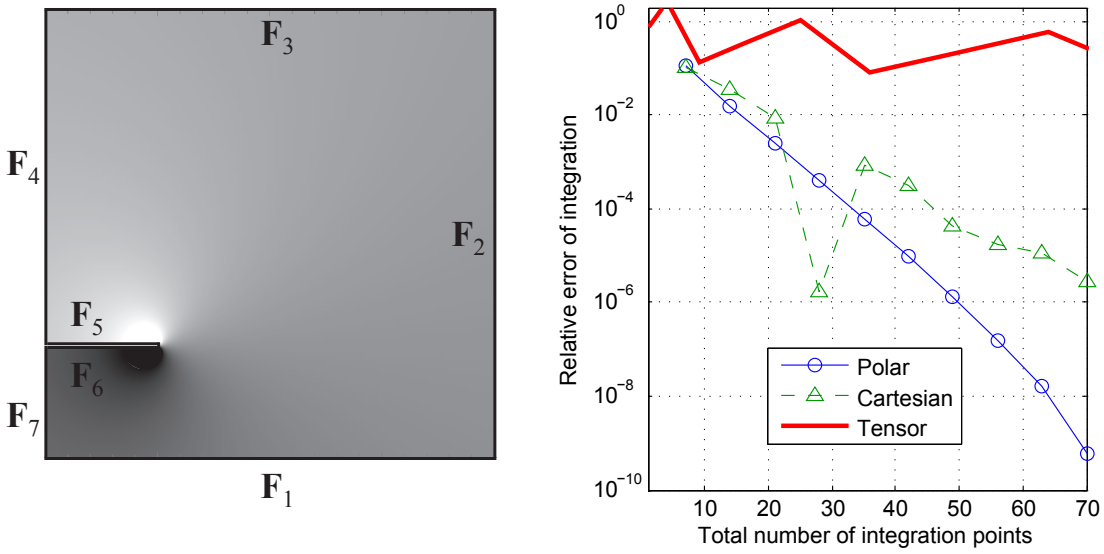

(a) (b)

Fig. 6: Error in numerical integration of $f(r,\theta) = \frac{1}{\sqrt{r}} \sin\frac{\theta}{2}$ over a biunit square centered at $x, y = (0.5, 0.5)$. P, $\boldsymbol{F}_i$, and $f(r,\theta)$ (shaded in grey) are plotted in (a) and the error in numerical integration from three different methods is shown in (b) (see Figure 5 for a description). Note in (a) that $f(r,\theta)$ is discontinuous at $y = 0 \cap x < 0$ and becomes unbounded at the origin.

One function whose implementation is not obvious is the function to calculate $\boldsymbol{a}_i$ and b_i from the vertices of the hyperplane. These quantities must be calculated such that the normal is oriented outward from the polytope. A simple method to do this is to ensure that the vertices of the polytope are given in counterclockwise orientation when standing outside the polytope. Then, we calculate $\boldsymbol{a}_i$ and b_i using the equation

$$\det \begin{vmatrix} x_1 & x_2 & \dots & x_d & 1 \\ x_{11} & x_{12} & \dots & x_{1d} & 1 \\ x_{21} & x_{22} & \dots & x_{2d} & 1 \\ \vdots & \vdots & \ddots & \vdots & \vdots \\ x_{d1} & x_{d2} & \dots & x_{dd} & 1 \end{vmatrix} = 0, \tag{23}$$

where x_{ij} is the j-th coordinate of the i-th vertex of d linearly independent vertices that lie in the hyperplane of interest. The determinant gives $a_{i1}x_1 + a_{i2}x_2 \cdots + a_{id}x_d = b_i$ with the proper orientation.

Algorithm 1 Integration of polynomial over arbitrary polytope using method of Section 2

```
Determine the dimension, d, of the polytope
Determine m, the number of hyperplanes
for i = 1 to m do
    Calculate a_i and b_i for the m hyperplanes
end for
Break f(x) into q homogeneous polynomials
Int ← 0
for j = 1 to q do
    h ← 0
    for i = 1 to m do
        g ← Call Alg. 2 with a_i, b_i, d − 1 and f_j(x)
        h ← h + b_i/‖a_i‖ × g
    end for
    h ← h/(d + j)
    Int ← Int + h
end for
return Int
```

5 Results

The implementation described in Section 4 is applied to a wide variety of test problems to demonstrate its versatility and ability to accurately and efficiently integrate polynomial functions. A selection of these test problems are presented in this section. First, we will demonstrate the method in Section 3 for a simple convex polygon. Then, we will apply our algorithm to more complicated shapes in Sections 5.3 through 5.5. Results are verified with `LattE integrale` 1.7.2 [12], a code capable of generating exact, fractional expressions for integrals of polynomials over convex polytopes [13, 14].

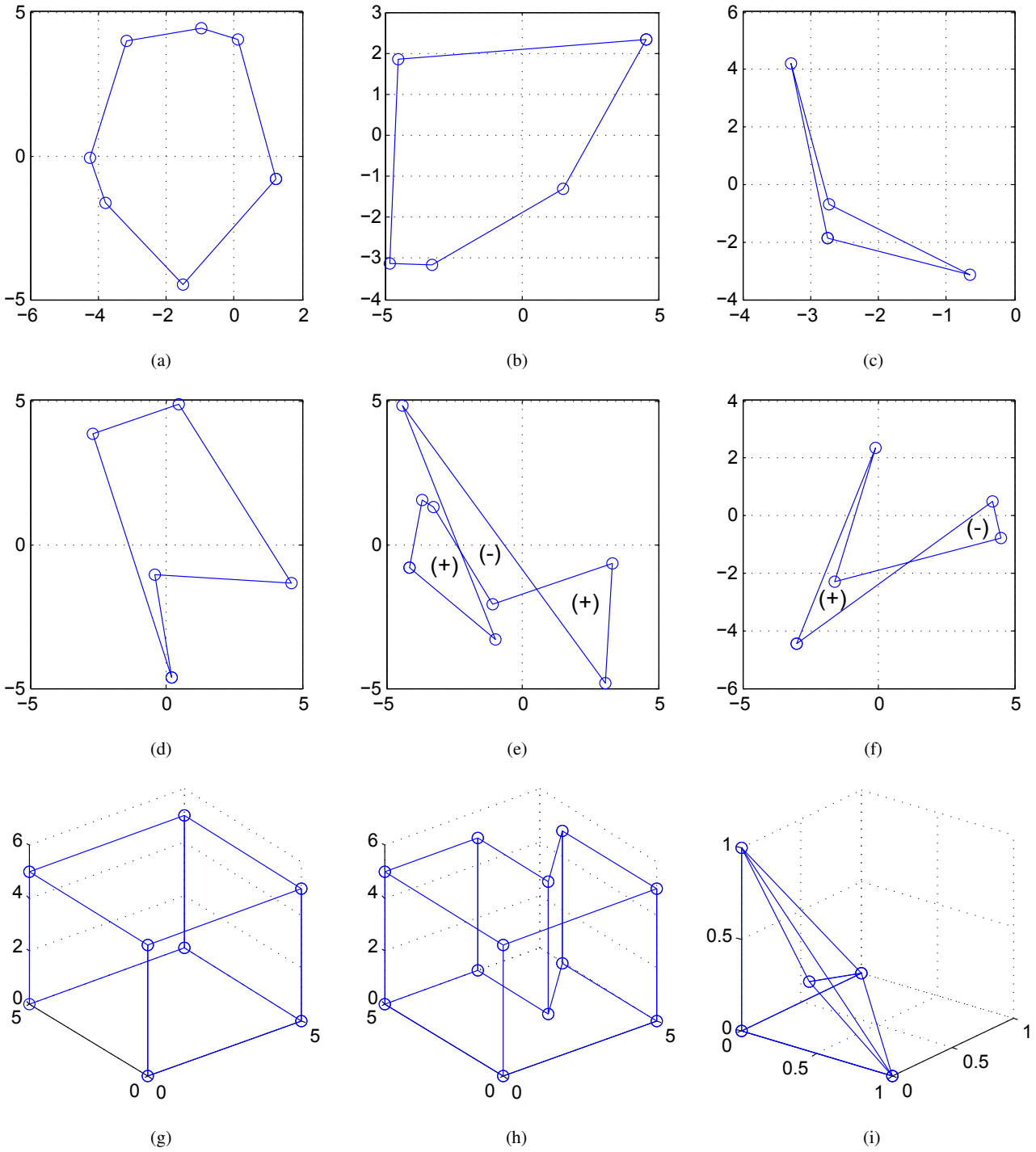

Fig. 7: Tests on polygons and polyhedra. (a) and (b) represent convex polygons. (c) and (d) represent simple nonconvex polygons. (e) and (f) represent non-simple nonconvex polygons. Positive and negative areas in (e) and (f) are represented by the (+) and (-) symbols, respectively. (g), (h), and (i) represent polyhedra with (h) and (i) being nonconvex. In cases (a) - (f), the homogeneous polynomial $x^2 + xy + y^2$ is integrated over the polygon. In cases (g) - (i), the homogeneous polynomial $x^2 + xy + y^2 + z^2$ is integrated over the polyhedron.

Algorithm 2 Futher reduction of integration using method of Section 3

Require: $\boldsymbol{a}_i$, b_i, d and $f(\boldsymbol{x})$
  $g \leftarrow 0$
  Determine $\boldsymbol{x}_0$ from $\boldsymbol{a}_i$ and b_i
  Determine $\tilde{\boldsymbol{x}}$ and $\tilde{d}$, the specific variables and number of variables present in $f_j(\boldsymbol{x})$
  for $i = 1$ to $\tilde{d}$ **do**
    Calculate $\frac{\partial f(\tilde{\boldsymbol{x}})}{\partial \tilde{x}_i}$
    $g \leftarrow g +$ Call Alg. 2 with $\boldsymbol{a}_i$, b_i, d and $(x_0)_i \frac{\partial f(\tilde{\boldsymbol{x}})}{\partial \tilde{x}_i}$
  end for
  for $j = 1$ to m **do**
    if $\boldsymbol{F}_i \cap \boldsymbol{F}_j \neq \emptyset$ **then**
      Calculate d_{ij}
      if $\boldsymbol{F}_{ij} = \boldsymbol{v}_{ij}$ **then** ▷ Determine if $\boldsymbol{F}_{ij}$ is a vertex
        $g \leftarrow g + d_{ij} f(\boldsymbol{v}_{ij})$
      else
        $g \leftarrow g +$ Call Alg. 2 with $\boldsymbol{a}_i$, b_i, $d-1$ and $d_{ij} f(\boldsymbol{x})$
      end if
    end if
  end for
  return g

5.1 Illustrative example

First, we apply our method to the integration of a homogeneous polynomial over a two-dimensional triangle. In this simple case, direct integration is carried out and compared to the result from our approach.

Consider the evaluation of the following two-dimensional integral:

$$I = \int_P xy \, dxdy \tag{24a}$$

over the triangle described by

$$P := \left\{ (x, y) \in \mathbb{R}^2 \mid x + y \leq 2, x \geq y, x \geq 0 \right\}. \tag{24b}$$

Direct integration gives the exact result: $I = 1/3$.

On setting $\boldsymbol{F}_1 := P \cap \{x + y \leq 2\}$, we have

$$\frac{b_1}{\|\boldsymbol{a}_1\|} \int_{\boldsymbol{F}_1} xy \, d\mu = \sqrt{2} \int_{\boldsymbol{F}_1} xy \, d\mu.$$

Selecting $x_0 = (2, 0)$ and using (10), the integration over $\boldsymbol{F}_1$ reduces to

$$\sqrt{2} \int_{\boldsymbol{F}_1} xy \, d\mu = \frac{\sqrt{2}}{2 + 2 - 1} \left(\sqrt{2} + 2 \int_{\boldsymbol{F}_i} y \, d\mu \right).$$

On reapplying (10), we obtain

$$\sqrt{2} \int_{\boldsymbol{F}_1} xy \, d\mu = \frac{\sqrt{2}}{3} \left(\sqrt{2} + \frac{2}{2 + 2 - 2} \left(\sqrt{2} \right) \right) = \frac{4}{3}.$$

Now, set $\boldsymbol{F}_2 := P \cap \{x \geq y\}$ and $\boldsymbol{F}_3 := P \cap \{x \geq 0\}$. For both of these hyperplanes, $b_i / \|\boldsymbol{a}_i\| = 0$. Therefore, on applying (7), we get

$$I = \frac{1}{2 + 2} \left(\frac{4}{3} \right) = \frac{1}{3},$$

which matches the exact value of the integral.

5.2 Application to convex polygons

Table 1: Vertices of polygons used as test cases.

Polygon in Fig. 7	Vertex	x	y
(a)	1	1.220	−0.827
	2	−1.490	−4.503
	3	−3.766	−1.622
	4	−4.240	−0.091
	5	−3.160	4.000
	6	−0.981	4.447
	7	0.132	4.027
(b)	1	4.561	2.317
	2	1.491	−1.315
	3	−3.310	−3.164
	4	−4.845	−3.110
	5	−4.569	1.867
(c)	1	−2.740	−1.888
	2	−3.292	4.233
	3	−2.723	−0.697
	4	−0.643	−3.151
(d)	1	0.211	−4.622
	2	−2.684	3.851
	3	0.468	4.879
	4	4.630	−1.325
	5	−0.411	−1.044
(e)	1	−4.165	−0.832
	2	−3.668	1.568
	3	−3.266	1.279
	4	−1.090	−2.080
	5	3.313	−0.683
	6	3.033	−4.845
	7	−4.395	4.840
	8	−1.007	−3.328
(f)	1	−3.018	−4.473
	2	−0.103	2.378
	3	−1.605	−2.308
	4	4.516	−0.771
	5	4.203	0.478

We apply our algorithm to a variety of convex polygons, and compare our numerical results to exact results from `LattE`. Random 2D polygons are constructed using a random number generator. The number of facets is first decided by generating a random integer between 3 and 10. Then random points are selected within $(-5, 5) \times (-5, 5) \subset \mathbb{R}^2$. These random points are truncated at the thousands

Table 2: Vertices of polyhedra used as test cases.

Polyhedron in Fig. 7	Vertex	x	y	z
(g)	1	0	0	0
	2	5	0	0
	3	5	5	0
	4	0	5	0
	5	0	0	5
	6	5	0	5
	7	5	5	5
	8	0	5	5
(h)	1	0	0	0
	2	5	0	0
	3	5	4	0
	4	3	2	0
	5	3	5	0
	6	0	5	0
	7	0	0	5
	8	5	0	5
	9	5	4	5
	10	3	2	5
	11	3	5	5
	12	0	5	5
(i)	1	0	0	0
	2	1	0	0
	3	0	1	0
	4	0	0	1
	5	0.25	0.25	0.25

place to allow for fractional representation in `LattE`. The points are verified to form a convex polygon, then Algorithms 1 and 2 are executed for the homogeneous polynomial $x^2 + xy + y^2$. Here, we provide results for two different polygons, which are shown in Figures 7a and 7b. The vertices of the polygons are listed in Table 1.

To verify the accuracy of our method, we invoke the Symbolic Math Toolbox as part of MATLAB R2014a™, which allows for exact calculation of these integrals using our algorithm. Results from integrating these polygons are listed in Table 3, along with exact results from `LattE`. For both test cases, our results exactly match those obtained using `LattE`.

5.3 Application to simple nonconvex polygons

Next, we apply our algorithm to a variety of simple (non-intersecting) nonconvex polygons, and compare our numerical results to exact results from `LattE`. Random 2D, simple, nonconvex polygons are generated similarly to those in Section 5.2, then Algorithms 1 and 2 are executed for the homogeneous polynomial $x^2 + xy + y^2$. Results are demonstrated for two different polygons, illustrated in Figures 7a and 7b. The vertices of the polygons are listed in Table 1.

Results from integration using the MATLAB Symbolic Math Toolbox and exact integration from `LattE` are listed in Table 3. Since `LattE` is only capable of integration on convex polytopes, our nonconvex polygons are integrated in `LattE` by decomposing the nonconvex polygon into an identical collection of convex polygons, performing integration on these polygons, then summing the results. No error is introduced by this decomposition since results from `LattE` are exact. For both test cases, our results exactly match those obtained using `LattE`.

5.4 Application to nonsimple nonconvex polygons

Our approach is also able to handle integration of nonconvex polygons where the boundary facets are intersecting, provided we define positive and negative areas of the polygon. Negative areas of the polygon are defined by a region of the polygon which has been intersected by boundary facets an odd number of times. Positive areas are defined by the areas which have not been intersected and areas which have been intersected an even number of times. In this section, we provide two examples that demonstrate this capability.

The three polygons are developed analogously to those in Section 5.3 and run with the same homogeneous polynomial. These polygons, along with definitions of positive and negative areas on them, are shown in Figures 7c and 7d. The vertices of these polygons are listed in Table 1. As with the convex polygons and the simple nonconvex polygons, the results (listed in Table 3) exactly match those obtained using `LattE`.

5.5 Application to nonconvex polyhedra

Finally, our algorithm was applied to a range of different convex and nonconvex polyhedra. The test cases presented here include a cube, a concave polyhedron consisting of a cube with a notch removed from it, and a tetrahedron with a tetrahedron carved from a face to make the polyhedron nonconvex. Rather than selecting random vertices and boundary facets as was done in Sections 5.3 and 5.4, we chose to manually select the vertices of this polyhedron. The vertices of these polyhedra are listed in Table 2 and illustrations are provided in Figures 7g, 7h, and 7i. The homogeneous polynomial $x^2 + xy + y^2 + z^2$ is integrated over the polyhedra. As demonstrated in Table 3, present results matched exactly those produced in `LattE`.

Table 3: Results of integrating a homogeneous polynomial over the polytopes shown in Figure 7 using `LattE` [12] and the present method.

Polytope in Fig. 7	Exact Result [12]	Present Method
(a)	$\frac{2031627344735367}{8000000000000}$	$\frac{2031627344735367}{8000000000000}$
(b)	$\frac{517091313866043}{1600000000000}$	$\frac{517091313866043}{1600000000000}$
(c)	$\frac{147449361647041}{8000000000000}$	$\frac{147449361647041}{8000000000000}$
(d)	$\frac{180742845225803}{1000000000000}$	$\frac{180742845225803}{1000000000000}$
(e)	$\frac{1633405224899363}{24000000000000}$	$\frac{1633405224899363}{24000000000000}$
(f)	$\frac{88161333955921}{3000000000000}$	$\frac{88161333955921}{3000000000000}$
(g)	$\frac{15625}{4}$	$\frac{15625}{4}$
(h)	$\frac{33835}{12}$	$\frac{33835}{12}$
(i)	$\frac{37}{960}$	$\frac{37}{960}$

5.6 Integration of arbitrary polynomials

While the methods introduced in the previous sections are of great utility when the integrand is known explicitly, often times the integrand is not known, and can only be evaluated at points within the domain. To handle this situation, Mousavi and Sukumar [7] developed a method to integrate arbitrary, unknown polynomials up to degree q by taking advantage of the properties of homogeneous functions and solving a small system of linear equations. Here, we demonstrate the method is equally valid for both convex and non-convex polytopes.

Integrating a polynomial using (8) requires the polynomial to be known *a priori*. However, simple manipulation of (8) leads to

$$\sum_{j=0}^{\hat{q}}(d+j)\int_P \hat{f}_j(\boldsymbol{x})\,d\boldsymbol{x} = \sum_{i=1}^{m}\frac{b_i}{\|\boldsymbol{a}_i\|}\int_{\boldsymbol{F}_i}\sum_{j=0}^{\hat{q}}\hat{f}_j(\boldsymbol{x})\,d\sigma. \quad (25)$$

Note that

$$\int_P g(\boldsymbol{x})\,d\boldsymbol{x} = \sum_{j=0}^{\hat{q}}\int_P \hat{f}_j(\boldsymbol{x})\,d\boldsymbol{x} \quad (26)$$

gives the quantity of interest. The integral $\int_{\boldsymbol{F}_i}\sum_{j=0}^{\hat{q}}\hat{f}_j(\boldsymbol{x})\,d\sigma$ can also be computed using Gauss quadrature by sampling points within the domain $\boldsymbol{F}_i$, i.e., without knowing the integrand explicitly. Thus, the right side of (25) can be evaluated for any arbitrary polynomial, provided sufficient number of quadrature points are used. Noting that homogeneous functions of degree q have the property $f(\lambda\boldsymbol{x}) = \lambda^q f(\boldsymbol{x})$, we can manipulate (25) to obtain

$$\sum_{j=0}^{\hat{q}}\lambda^j(d+j)I_j = Q(\lambda), \quad (27a)$$

where

$$I_j := \int_P \hat{f}_j(\boldsymbol{x})\,d\boldsymbol{x}, \quad (27b)$$

$$Q(\lambda) := \sum_{i=1}^{m}\frac{b_i}{\|\boldsymbol{a}_i\|}\int_{\boldsymbol{F}_i}\sum_{j=0}^{\hat{q}}\hat{f}_j(\lambda\boldsymbol{x})\,d\sigma. \quad (27c)$$

This provides an arbitrary number of equations that are formed by varying the value of λ. As before, the right side of the equation can be evaluated through sampling points within $\boldsymbol{F}_i$. Choosing $\hat{q}+1$ values of λ results in a $(\hat{q}+1)\times(\hat{q}+1)$ system of equations that can be used to solve each term of (26), without explicitly knowing each term, $\hat{f}_j(x)$. On choosing $\hat{q}+1$ distinct values for λ, we can write (27) as

$$\sum_{j=0}^{\hat{q}}\lambda_k^j(d+j)I_j = Q(\lambda_k) \quad (28)$$

for $k = 1,\ldots,\hat{q}+1$.

This approach is used to integrate the polynomial $f(x) = x^3+xy^2+y^2+x$ over the polygons shown in Figure 7a and Figure 7c. The polynomial $f(x)$ contains monomials up to degree three. Therefore, the integral of each monomial can be determined through the solution of a 4×4 linear system, defined by (28). We choose $\lambda = (0.25, 0.5, 0.75, 1)$ to compute the 4×4 system matrix and to determine the location of the quadrature points within the domain of the boundary facets.

With this choice of λ for the polygon shown in Figure 7a, (28) becomes

$$\begin{bmatrix} 2 & \frac{3}{4} & \frac{1}{4} & \frac{5}{64} \\ 2 & \frac{3}{2} & 1 & \frac{5}{8} \\ 2 & \frac{9}{4} & \frac{9}{4} & \frac{135}{64} \\ 2 & 3 & 4 & 5 \end{bmatrix}\begin{bmatrix} I_1 \\ I_2 \\ I_3 \\ I_4 \end{bmatrix} = \begin{bmatrix} -\frac{11550135635909446173}{2560000000000000000} \\ -\frac{9080398944401774173}{32000000000000000} \\ -\frac{251474206771886854671}{2560000000000000000} \\ -\frac{9628722192185938173}{4000000000000000} \end{bmatrix}.$$

Solving for $I_1,\ldots,I_4$, we obtain

$$\begin{bmatrix} I_1 \\ I_2 \\ I_3 \\ I_4 \end{bmatrix} = \begin{bmatrix} 0 \\ -\frac{99066199641}{2000000000} \\ \frac{582878710330541}{4000000000000} \\ -\frac{11365839835662102173}{200000000000000000} \end{bmatrix}.$$

Using (26), we calculate $\int_P g(\boldsymbol{x})\,d\boldsymbol{x} \approx -472.105$. This result matches integration of the monomials using (8).

For the polygon in Figure 7c, the linear system that is obtained from (28) is:

$$\begin{bmatrix} 2 & \frac{3}{4} & \frac{1}{4} & \frac{5}{64} \\ 2 & \frac{3}{2} & 1 & \frac{5}{8} \\ 2 & \frac{9}{4} & \frac{9}{4} & \frac{135}{64} \\ 2 & 3 & 4 & 5 \end{bmatrix} \begin{bmatrix} I_1 \\ I_2 \\ I_3 \\ I_4 \end{bmatrix} = \begin{bmatrix} -\frac{1005647136056845793}{256000000000000000} \\ -\frac{659018727981237793}{32000000000000000} \\ -\frac{16790442429180948411}{256000000000000000} \\ -\frac{617991551841433793}{4000000000000000} \end{bmatrix}.$$

Again, solving for $I_1, \ldots, I_4$ gives

$$\begin{bmatrix} I_1 \\ I_2 \\ I_3 \\ I_4 \end{bmatrix} = \begin{bmatrix} 0 \\ -\frac{22047837983}{6000000000} \\ \frac{22814962939549}{4000000000000} \\ -\frac{665155727633629793}{20000000000000000} \end{bmatrix}.$$

Summing each I_k, we obtain $\int_P g(\boldsymbol{x})\, d\boldsymbol{x} \approx -31.229$. As with the convex polygon, the result matches integration of the monomials using (8).

6 Concluding remarks

In this paper, we applied Euler's homogeneous function theorem and Stokes's theorem to devise a method for reducing integration of homogeneous polynomials over arbitrary convex and nonconvex polytopes to integration over the boundary facets of the polytope. Additionally, we also demonstrated that the same tools could be used to further reduce the integration if partial derivatives of the homogeneous function exist. For homogeneous polynomials, integration can ultimately be reduced to function evaluation at the vertices of the polytope.

We implemented our method and presented several numerical examples that showcased its capabilities. In addition to integrating homogeneous polynomials over irregular convex and nonconvex polytopes, we also demonstrated how the method could be applied to nonsimple nonconvex polytopes. Furthermore, we also successfully tested the approach for the integration of weakly singular functions in two dimensions over polygons with straight and curved facets. For all cases involving homogeneous polynomials that were tested, our results exactly matched the results obtained using the code `LattE` [12]. As part of future work, we plan to assess the proposed integration scheme in applications of the extended and embedded finite element methods, as well as Galerkin methods on polygons and polyhedra.

A Appendix

In this appendix, we describe an alternative method for reducing integration of homogeneous polynomials over polygons and polyhedra to lower-dimensional facets. Rather than using partial derivatives, as was done in Section 3, this method uses rotations to simplify integration over lower-dimensional facets. As with the method in Section 3, this method can be used to reduce integration to function evaluation at the vertices of the polytope.

To integrate the expression $f(\boldsymbol{x})$ in (7) (or $\hat{f}_j(\boldsymbol{x})$ in (8)) over the boundary facets, $\boldsymbol{F}_i$, the integral over $\mathbb{R}^d$ must first be transformed to an integral over $\mathcal{H}_i$, the hyperplane in which $\boldsymbol{F}_i$ lies. This can be accomplished through applying an affine transformation of the boundary facet such that it lies normal to one of the orthonormal coordinate axes in $\mathbb{R}^d$. In $\mathbb{R}^2$ and $\mathbb{R}^3$, this transformation is completed with a simple rotation matrix applied to both the vertices of the boundary facet and to the variables in the expression $f(\boldsymbol{x})$. Calculation of this rotation matrix in $\mathbb{R}^3$ is expedited by using Rodrigues's finite rotation formula [15]:

$$R = I + \hat{\boldsymbol{\omega}} \sin\theta + \hat{\boldsymbol{\omega}}^2 (1 - \cos\theta), \tag{29}$$

where θ is the desired angle of rotation, I is the 3×3 identity matrix, and $\hat{\boldsymbol{\omega}}$ is the skew-symmetric matrix whose components are:

$$\hat{\boldsymbol{\omega}} = \begin{pmatrix} 0 & -\omega_z & \omega_y \\ \omega_z & 0 & -\omega_z \\ -\omega_y & \omega_x & 0 \end{pmatrix}, \tag{30}$$

where ω_i $(i = x, y, z)$ give the components of the unit vector $\boldsymbol{\omega}$ about which the rotation occurs. This vector can be constructed for each $\boldsymbol{F}_i$ by the vector cross product

$$\boldsymbol{\omega} = \boldsymbol{a}_i / \|\boldsymbol{a}_i\| \times \boldsymbol{e}_z, \tag{31}$$

where $\boldsymbol{e}_z$ is a unit vector in the z-direction. When the transformation is applied to the expression $f(\boldsymbol{x})$, it is likely that the resulting equation will no longer be a homogeneous function. Instead, it will become a polynomial that can be integrated using (8). Applying this procedure d times to a d-dimensional polytope reduces integration to simple evaluation at the vertices of the polytope. Algorithm 3 describes an algorithm to implement this method. The examples in Section 5 were calculated using this method, and were shown to exactly match results using the method of Section 3. An example that illustrates this method follows.

Algorithm 3 Integration of polynomial over arbitrary polytope

```
Determine the dimension, d, of the polytope
Determine m, the number of hyperplanes
Break f(x) into q homogeneous polynomials
Int ← 0
for j = 1 to q do
    Determine the order, j, of f_j(x)
    if d > 1 then
        h ← 0
        for i = 1 to m do
            Calculate a_i and b_i for the hyperplane
            Build d-dimensional rotation matrix, R
            v'_i ← R v_i                    ▷ v_i: vertices of i-th facet
            x ← R^T x'
            g ←Call Algorithm 3 with f(R^T x') and v'_m
            h ← h + b_i/‖a_i‖ × g
        end for
        h ← h/(d + j)
        Int ← Int + h
    else
        Int ← Int + 1/(1 + j) [b_1 f(x_1)/a_1 + b_2 f(x_2)/a_2]
    end if
end for
return Int
```

A.1 Numerical example

We demonstrate the geometric method of degree-reduction using the example considered in Section 5.1: we evaluate the two-dimensional integral $I = \int_P xy\,dxdy$, where P is the triangle defined in (24b). Direct integration gives $I = 1/3$.

On setting $\boldsymbol{F}_1 := P \cap \{x + y \leq 2\}$, we have

$$\frac{b_1}{\|\boldsymbol{a}_1\|}\int_{\boldsymbol{F}_1} xy\,d\mu = \sqrt{2}\int_{\boldsymbol{F}_1} xy\,d\mu.$$

Next, we apply the rotation matrix

$$\boldsymbol{R} = \frac{1}{\sqrt{2}}\begin{bmatrix} 1 & -1 \\ 1 & 1 \end{bmatrix},$$

which aligns the hyperplane parallel to the x-axis (see Algorithm 1). The resulting transformed integral is:

$$\sqrt{2}\int_{\boldsymbol{F}_1} xy\,d\mu = \sqrt{2}\int_0^{\sqrt{2}} \left(1 - \frac{(x')^2}{2}\right) dx'.$$

Applying (8) yields

$$\sqrt{2}\int_0^{\sqrt{2}} \left(1 - \frac{(x')^2}{2}\right) dx' = \sqrt{2}\left[\sqrt{2} - \frac{\sqrt{2}}{3}\right] = \frac{4}{3}.$$

Now, set $\boldsymbol{F}_2 := P \cap \{x \geq y\}$ and $\boldsymbol{F}_3 := P \cap \{x \geq 0\}$. For both these hyperplanes, $b_i/\|\boldsymbol{a}_i\| = 0$. Therefore, on applying (7), we get

$$I = \frac{1}{2+2}\left(\frac{4}{3}\right) = \frac{1}{3},$$

which exactly matches the result from direct integration.

Acknowledgements The research support of the National Science Foundation through contract grant CMMI-1334783 to the University of California at Davis is gratefully acknowledged.

References

1. T. P. Fries and T. Belytschko. The extended/generalized finite element method: An overview of the method and its applications. *Int. J. Numer. Meth. Engng.*, 84(3):253–304, 2010.
2. Y. Sudhakar J. P. Moitinho de Almeida and W. A. Wall. An accurate, robust, and easy-to-implement method for integration over arbitrary polyhedra: Application to embedded interface methods. *J. Comp. Phys.*, 273:393–415, 2014.
3. Y. Sudhakar and W. A. Wall. Quadrature schemes for arbitrary convex/concave volumes and integration of weak form in enriched partition of unity methods. *Comput. Methods Appl. Mech. Engrg.*, 258:39–54, 2013.
4. D. Schillinger and M. Reuss. The finite cell method: A review in the context of higher-order structural analysis of CAD and image-based geometric models. *Arch. Comput. Methods Engrg.*, 2014. DOI: 10.1007/s11831-014-9115-y.
5. L. Beirao da Veiga, F. Brezzi, A. Cangiani, G. Manzini, L. D. Marini, and A. Russo. Basic principles of virtual element methods. *Math. Models Methods Appl. Sci.*, 23:199–214, 2013.
6. L. Chen. Equivalence of weak Galerkin methods and virtual element methods for elliptic equations. 2015. Preprint available at `http://arxiv.org/abs/1503.04700`.
7. S. E. Mousavi and N. Sukumar. Numerical integration of polynomials and discontinuous functions on irregular convex polygons and polyhedrons. *Comput. Mech.*, 47:535–554, 2011.
8. J. B. Lasserre. Integration on a convex polytope. *Proc. Amer. Math. Soc.*, 126(8):2433–2441, 1998.
9. M. E. Taylor. *Partial Differential Equations: Basic Theory*. Springer-Verlag, New York, 1996.
10. J. B. Lasserre. An analytical expression and an algorithm for the volume of a convex polyhedron in $\mathbb{R}^n$. *J. Optim. Theory and Appl.*, 39(3):363–377, 1983.
11. J. B. Lasserre. Integration and homogeneous functions. *Proc. Amer. Math. Soc.*, 127(3):813–818, 1999.
12. V. Baldoni, N. Berline, J. A. De Leora, B. Dutra, M. Köppe, S. Moreinis, G. Pinto, M. Vergne, and J. Wu. *A User's Guide for `LattE integrale` v1.7.2*. Department of Mathematics, University of California, Davis, CA 95616, October 2014. Available at `http://www.math.ucdavis.edu/~latte`.
13. V. Baldoni, N. Berline, J. A. De Loera, M. Köppe, and M. Vergne. How to integrate polynomials over simplices. *Math. Comp.*, 80:297–325, 2011.
14. J. A. De Loera, B. Dutra, M. Köppe, S. Moreinis, G. Pinto, and J. Wu. Software for exact integration of polynomials over polyhedra. *Comput. Geom.*, 46(3):232–252, 2013.
15. M. F. Beatty. Vector analysis of finite rigid rotations. *J. Appl. Mech.*, 44(3):501–502, 1977.